



UNIVERSITY OF LEEDS

This is a repository copy of *The influence of solution environment on the nucleation kinetics and crystallisability of para-aminobenzoic acid.*

White Rose Research Online URL for this paper:  
<http://eprints.whiterose.ac.uk/106276/>

Version: Accepted Version

---

**Article:**

Turner, TD, Corzo, DM, Toroz, D et al. (5 more authors) (2016) The influence of solution environment on the nucleation kinetics and crystallisability of para-aminobenzoic acid. *Physical Chemistry Chemical Physics*, 18 (39). pp. 27507-27520. ISSN 1463-9076

<https://doi.org/10.1039/c6cp04320h>

---

(c) 2016, Royal Society of Chemistry. This is an author produced version of a paper published in *Physical Chemistry Chemical Physics*. Uploaded in accordance with the publisher's self-archiving policy.

**Reuse**

Unless indicated otherwise, fulltext items are protected by copyright with all rights reserved. The copyright exception in section 29 of the Copyright, Designs and Patents Act 1988 allows the making of a single copy solely for the purpose of non-commercial research or private study within the limits of fair dealing. The publisher or other rights-holder may allow further reproduction and re-use of this version - refer to the White Rose Research Online record for this item. Where records identify the publisher as the copyright holder, users can verify any specific terms of use on the publisher's website.

**Takedown**

If you consider content in White Rose Research Online to be in breach of UK law, please notify us by emailing [eprints@whiterose.ac.uk](mailto:eprints@whiterose.ac.uk) including the URL of the record and the reason for the withdrawal request.



[eprints@whiterose.ac.uk](mailto:eprints@whiterose.ac.uk)  
<https://eprints.whiterose.ac.uk/>

**The Influence of Solution Environment on the Nucleation Kinetics and Crystallisability  
of Para-aminobenzoic Acid**

**T. D. Turner, D. M. C. Corzo, ‡D. Toroz, A. Curtis, †M. M. Dos Santos, R. B.  
Hammond, X. Lai, K. J. Roberts\***

<sup>a</sup>Institute for Process Research and Development, School of Chemical and Process  
Engineering, University of Leeds, Woodhouse Lane, Leeds, LS2 9JT

*‡ Department of Chemistry, Imperial College London, London SW7 2AZ*

<sup>†</sup>Centro de Tecnologia, Escola de Química, Universidade Federal do Rio de Janeiro, Rio de  
Janeiro, Brasil, CEP 21941-909

\* Corresponding Author

*‡ †* Current Address

**Keywords:** nucleation kinetics and mechanism, crystal growth, crystallisability, solvent effects, optical turbidometric measurements, poly-thermal nucleation studies, KBHR method, solution ideality, solvation free energies, molecular dynamics, meta-stable zone width, para amino benzoic acid.

## Abstract

The influence of solvent type on the solution thermodynamics, nucleation-kinetics and crystal growth of alpha para-aminobenzoic acid (PABA) crystallising from supersaturated ethanol, acetonitrile and water solutions, is examined using poly-thermal analysis of the metastable zone width. Application of a recently proposed model for analysis of crystallisation kinetics (J. Cryst. Growth, 312 (2010) 698–704) indicates a solvent and concentration dependence of the nucleation mechanism and key nucleation parameters for the alpha form of PABA. The mechanism of nucleation is found to change from instantaneous to progressive with decreasing concentration and also when changing the solvent from ethanol to acetonitrile to water. The dependence of the nucleation mechanism is correlated to the kinetic component of the nucleation rate through calculated number concentrations of instantaneously nucleated crystallites, which increase from  $1.40 \times 10^9 \text{ m}^{-3}$  in ethanol to  $1.08 \times 10^{10} \text{ m}^{-3}$  in acetonitrile to  $2.58 \times 10^{10} \text{ m}^{-3}$  in water. This in combination with low calculated values of interfacial tension between 1.13 and 2.71  $\text{mJ/m}^{-2}$ , supports the conclusion that the kinetic component of the nucleation rate is more limiting when crystallising PABA from ethanol solutions in comparison to water solutions. This finding is further supported by molecular dynamics simulations of the solvation free energy of PABA, which is found to be greatest in water, -42.4 kJ/mol and lowest in ethanol, -58.5 kJ/mol.

## 1. Introduction

Cooling crystallisation from saturated solutions is widely used in the pharmaceutical, crop protection, energy and food industries as a methodology for effecting the phase separation and purification of target compounds<sup>1</sup>. Underpinning the process of crystallisation is nucleation, the intermediary step between the solution and solid-states, which as such can be considered to be crucial in determining the characteristic physical and chemical properties of the final solid form<sup>2</sup>. The influence of the solution state structure in directing the nucleation and growth processes is not fully understood particularly for organic molecular materials. However, it is known that the solution chemistry of the solvent can strongly influence the molecular self-assembly, nucleation and growth processes and, hence, can impact on the morphology, habit and size distribution of particles in the resultant crystalline phase<sup>3 4 5</sup>. Davey<sup>6</sup> proposed that the de-solvation rates of a solute molecule can be the rate-limiting step for both nucleation and crystal growth; this was recently highlighted by comparing the free energy of solvation of the carboxylic acid dimer of para-aminobenzoic acid (PABA) in various solvents, to attachment frequency calculated from isothermal nucleation studies<sup>7</sup>. From this it is clear that solution chemistry can change the interfacial energy at the liquid-solid interface, either of a cluster of molecules or a crystallite surface. However, for organic materials further studies are required to link the solution chemistry of a target molecule to the measured nucleation kinetics. A comprehensive review of nucleation rates and the potential relationship to solution chemistry and self-assembly has been recently provided by Davey et al<sup>8</sup>.

Understanding, characterising and defining the nucleation process together with its underpinning thermodynamic and kinetic aspects is a necessary component in the design of crystallisation processes. Recent studies have shown that nucleation kinetic parameters can

be derived from the probability distribution of induction times (time taken for a system to crystallise while under non-kinetic supersaturation conditions) as observed from measurements of induction times at a set temperature and hence supersaturation (isothermal method), and these have been related to the mechanisms by which critical nuclei form in supersaturated solutions<sup>9</sup>. The relationship between induction time and supersaturation can be used to calculate nucleation kinetic parameters, such as interfacial tension and the methodology has been successfully applied to organic materials<sup>7, 10, 11</sup>.

Crystallisation parameters can also be obtained by observing the effect of cooling rate on the measured achievable undercooling (polythermal method) which has also been used to study crystallisation due to the fundamental connection between the meta-stable zone width (the difference between the equilibrium solubility and crystallisation temperatures,  $\Delta T_c$ ) and the crystallite properties<sup>12,13,14,15,16</sup>. This method relates  $\Delta T_c$  to the cooling rate,  $q$ , to calculate nucleation kinetics and information about crystallite growth. The most common interpretation of  $\Delta T_c$  vs  $q$  data is using the empirical Nyvlt expressions<sup>17, 18</sup>, however Kubota<sup>19</sup> and Sangwal<sup>20, 21</sup> have recently re-interpreted these equations in order to derive more physically meaningful parameters. These poly-thermal approaches have been comprehensively reviewed and applied to paracetamol-ethanol solutions by Mitchell et al through which the key kinetic parameters were derived<sup>22</sup>.

More recently a more rigorous theoretical approach has led to further development of the polythermal method by Kaschiev, Borrisova, Hammond and Roberts<sup>23, 24, 25</sup> (KBHR). The KBHR approach allows determination of important nucleation parameters providing also insight into the nucleation and growth mechanisms of crystallites. This approach has been recently applied to methyl stearate crystallising from kerosene from which the interfacial tension was determined and cross-validated using an isothermal methodology<sup>25</sup>.

These advances have provided significant mechanistic insight together with key kinetic parameters for both nucleation and growth and in this paper this approach is applied to para-amino benzoic acid (PABA), shown in Figure 1.

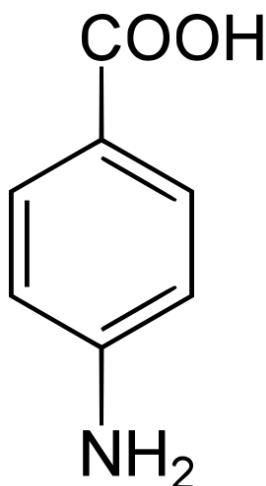


Figure 1 Chemical structure of para-amino benzoic acid

PABA contains carboxylic acid and amino functional groups and as such exhibits some of the molecular scale characteristics of pharmaceuticals and their pre-cursors<sup>26,27,28,29,30,31,32,33</sup>. This work focuses on the crystallisation of the alpha polymorphic form of PABA as crystallised from three solvents; ethanol, acetonitrile and water. Preliminary studies of alpha PABA crystallising from ethanol have been previously published<sup>34</sup>. This paper extends this work by contrasting this with data collected using different solvents; acetonitrile and water. Through the identification of the nucleation mechanism and the characterisation of key nucleation and growth parameters for three different solvents, the aim of this study is to understand how changes in the solvation environment and crystallisation supersaturation direct the crystallisation of PABA and impact on its physical form.

## 2. Theory

### 2.1. Assessment of solubility

A compound's molar solubility,  $x$ , is the concentration of the solute at equilibrium and can be related to the solubility of the ideal state  $x_{ideal}$ . through its activity coefficient,  $\gamma$ , given by expression (1), this was derived by equating the activities of the ideal and non-ideal states from the normal definition of activity.

$$\gamma = \frac{x_{ideal}}{x} \quad \text{(Equation 1)}$$

The ideal model solid-liquid equilibrium with the assumption of negligible contribution of heat capacity,  $C_p$ , can be expressed as

$$\ln(x) = \frac{\Delta H_{fus}}{R} \left[ \frac{1}{T} - \frac{1}{T_m} \right] \quad \text{(Equation 2)}$$

where  $R$  is the ideal gas constant,  $\Delta H_{fus}$  is the enthalpy of fusion,  $T$  is temperature and  $T_m$  is the melting temperature of the solute<sup>35</sup>. Assuming non-ideal behaviour the van't Hoff equation can also be expressed as;

$$\ln(x) = -\frac{\Delta H_{diss}}{RT} + \frac{\Delta S_{diss}}{R} \quad \text{(Equation 3)}$$

where  $\Delta H_{diss}$  and  $\Delta S_{diss}$  are the enthalpy and entropy of dissolution respectively. The enthalpy reported in this study refers to the enthalpic change on dissolving a mole of a substance in an infinite amount of saturated solution<sup>36</sup>. A solute's solvation enthalpy,  $\Delta H_{solv}$ , is derived through  $\Delta H_{diss}$  through the enthalpy of sublimation of the solute  $\Delta H_{sub}$ , where  $\Delta H_{sub}$  can be estimated through the crystalline materials lattice energy,  $E_{latt}$  (for the PABA alpha polymorph this was found to be  $102.6 \text{ KJ/mol}^{-1}$ )<sup>37</sup>. For a full derivation of terms please see the supplementary material.

## 2.2. Assessment of Crystallisation Kinetics using the KBHR Methodology

The assessment of crystallisation kinetics was carried out through the application of the KBHR method. Using this approach the average values of  $T_{dis}$  and  $T_C$  allow calculation of the critical undercooling,  $\Delta T_c$ , using Equation 4, where  $T_e$  is the equilibrium solubility temperature and  $T_C$  is the crystallisation temperature;

$$\Delta T_c = T_e - T_C \text{ (Equation 4)}$$

A value of the relative critical undercooling,  $u_c$ , was calculated from Equation 5, where  $u_c$  is dimensionless.

$$u_c = \frac{\Delta T_c}{T_e} \text{ (Equation 5)}$$

Analysis of the slope from a linear regression of the measured  $u_c$  values versus cooling rate ( $q$ ) in ln-ln coordinates can be used to assess the nucleation mechanism; instantaneous or progressive. A slope of  $< 3$  is indicative of instantaneous nucleation, where nuclei all form at the same temperature, whereas a slope of  $>3$  being indicative of progressive nucleation whereby nuclei are formed at various temperatures leading to varying crystallite sizes<sup>38</sup>. To further scrutinise the dependence of  $u_c$  on  $q$ , the following inequalities must be met.

$$u_c < 0.1, au_c < 1 \text{ (Equation 6)}$$

The values of  $a$  were calculated using Equation 7;

$$a = \frac{\lambda}{k T_e} \text{ (Equation 7)}$$



where  $k$  is the Boltzmann constant and  $\lambda$  is the molecular latent heat of crystallisation, these values were averaged for each concentration over the various cooling rates.

### 2.2.1. Instantaneous Nucleation

For the case of instantaneous nucleation the value of  $q_0$ , a parameter related to the dependence of  $u_c$  on  $q$ , can be related to the concentration of crystallites,  $C_0$ , at the point of nucleation,  $t_0$ , through Equation 8,

$$q_0 = \left[ \frac{k_v C_0}{(n+1)^d \alpha_{det}} \right]^{\frac{1}{md}} (a)^n K_G T_e \quad \text{(Equation 8)}$$

Where  $n$  and  $m$  are growth exponents for the growth mechanism of the crystallites; where  $n = 1$  is associated with diffusion of solute across a crystal/solution interface, and  $n = 2$  indicates the presence of screw dislocations within the crystallite. The parameter  $m$  can take a value between 0.5 and 1, where  $m = 0.5$  indicates undisturbed diffusion of the solute to the crystal surface and  $m = 1$  indicates growth through diffusion of solute through a stagnant layer around the crystal<sup>39</sup>. The value of  $d$  is the dimensionality of the crystal growth i.e. 1 for needle like crystallites.  $K_G$  is the overall growth rate of the crystal (assumed as,  $K_G = 1 \times 10^{-8}$  m/s from growth studies of PABA crystals in ethanol) and  $K_v$  is the crystallite growth shape factor e.g.  $2A_0$  for needle like crystals (where  $A_0$  is the fixed needle cross-sectional area and in this case was taken from measured widths of crystallites recovered from the polythermal cooling experiments). The value of  $q_0$  can be obtained through a Nyvlt<sup>17,18</sup> type relationship by plotting the  $q$  vs  $u_c$  in ln-ln coordinates.

$$\ln q = \ln q_0 + (n + 1) \ln u_c \quad \text{(Equation 9)}$$

### 2.2.2. Progressive Nucleation

For the case of progressive nucleation the  $u_c$  ( $q$ ) dependence can be related through the number of crystallites at the detection point,  $N_{det}$ , which is described through the parameter  $q_0$ .

$$\ln(q) = \ln(q_0) + a_1 \ln(u_c) - \frac{a_2}{(1-u_c)u_c^2} \quad \text{(Equation 10)}$$

Plotting crystallisation parameters in  $\ln q$  vs  $u_c$  coordinates followed by a non-linear least squares fit of Equation 10 enables calculation of free parameters related to the nucleation and growth of crystallites, in this instance the fitting was carried out using OriginPro<sup>40</sup> software. In this  $a_1$  is a parameter related to the crystallite growth exponent's  $m$ ,  $n$  and  $d$ .

$$a_1 = 3 \quad \text{(Equation 11)}$$

The free parameter  $a_2$  is related to the nucleation parameter  $b$  and so can be used to calculate  $\gamma_{eff}$  where  $k_n$  is the nucleus shape factor ( $16\pi/3$  for a spherical nucleus),  $v_0$  is the molecular volume in the crystal.

$$a_2 = b = \frac{k_n v_0^2 \gamma_{eff}^3}{k T_e \lambda^2} \quad \text{(Equation 12)}$$

The final free parameter  $q_0$  takes into account growth and nucleation parameters, where  $K_J$  is the nucleation rate constant.

$$q_0 = \frac{V K_J T_e}{N_{det} 2b} \quad \text{(Equation 13)}$$

Following analysis of  $\gamma_{eff}$  through Equation 12 the critical nucleus radius,  $r^*$ , can be calculated through the following expression;

$$r^* = \frac{2 \gamma_{eff} v_0}{\lambda u} \quad \text{(Equation 14)}$$

the number of molecules within the critical nucleus,  $i^*$ , can be evaluated through Equation 15;

$$i^* = \frac{2 a_2 k T_e}{\lambda (u)^3} \quad (\text{Equation 15})$$

A flow chart summary of the KBHR analysis procedure is provided in Figure 2.

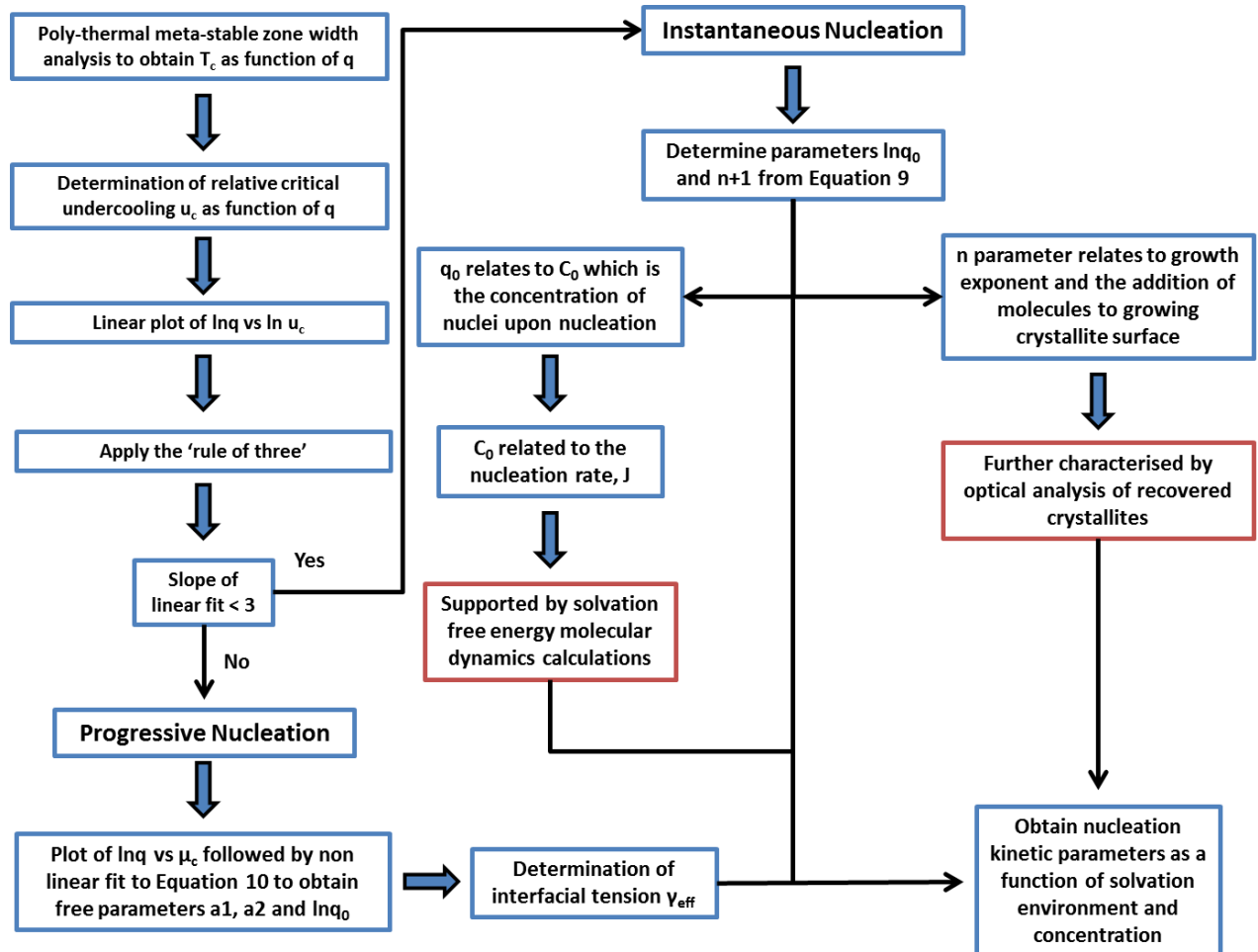


Figure 2: Flow chart indicating the procedure followed for application of the KBHR approach and 'the rule of three' analysis

### **3. Materials and Methods**

#### **3.1. Materials**

All experimental work was carried out using >99% PABA, 99.9% absolute ethanol, 99.9% acetonitrile all purchased from Sigma Aldrich and laboratory de-ionised water.

#### **3.2. Polythermal Data Collection**

##### **3.2.1. Apparatus**

Polythermal crystallisation experiments were carried out in a Technobis Crystal 16 unit<sup>41</sup>. This multiple reactor equipment allows sixteen 1.5ml vials, separated into 4 blocks, to be heated and cooled at specific rates by utilizing a combined Peltier heating and water bath cooling system. The vials were magnetically stirred using micro stirrer bars and the crystallisation process was monitored using a turbidometric system to detect the crystallisation and dissolution temperatures as a function of cooling and heating rates respectively.

##### **3.2.2. Sample Preparation**

Solutions of PABA in ethanol were prepared at 170, 180, and 190, 200 g/kg in acetonitrile at 54, 64.8, 75.6 and 86.4 g/kg and in de-ionised water at 6, 8, 10 and 12 g/kg of solvent on a 10 ml scale. PABA was weighed into vials using a balance accurate to four significant figures, followed by addition of the solvent by mass. The solutions were then stirred and heated to 50°C on a stirrer hotplate at 300rpm until the material dissolved to give a clear solution; the solutions were then transferred to the vials using pre-heated pipettes (50°C) to prevent unwanted crystallisation.

### 3.2.3. Polythermal Methodology

The solutions were heated and cooled in a pre-programmed cycle from 5°C to 50°C where the solutions were held at the higher temperature for one hour to allow complete dissolution of the solute, the rates of heating and cooling were 0.1, 0.3, 0.5, 0.7 and 1.0 °C / min with constant stirring by a micro magnetic stirrer at 300rpm.

Each cooling rate was repeated five times at each concentration to give good statistics for the measured dissolution and crystallisation temperatures,  $T_{\text{dis}}$  and  $T_{\text{C}}$  respectively.  $T_{\text{dis}}$  and  $T_{\text{C}}$  were obtained using a poly-thermal cooling profile where  $T_{\text{dis}}$  was determined when the transmission value reached 100% and  $T_{\text{C}}$  was determined as the point when the transmission percentage from the turbidity signal was observed to decrease below 90%.

### 3.2.4. Polythermal Data Analysis

Extrapolation of the measured  $T_{\text{dis}}$  to 0°C/min cooling rate was used to calculate the equilibrium dissolution temperature,  $T_{\text{e}}$ , and through this the solubility as a function of solute concentration and solvent choice. The values of  $T_{\text{e}}$  and  $T_{\text{C}}$  were then used to calculate the critical undercooling,  $\Delta T_{\text{c}}$  from Equation 4. This allowed the calculation of the relative critical undercooling,  $u_{\text{c}}$ , from Equation 5. It followed that for each solvent and the respective solute concentration, a plot of  $\ln u_{\text{c}}$  vs  $q$  was obtained, whereby the slope of a linear fit to the data points revealed the nucleation mechanism for the crystallisation process. This was followed by analysis using the procedure outlined in Figure 2, whereby the concentrations which revealed an instantaneous mechanism were further analysed using Equation 9, those which revealed a progressive mechanism Equation 10.

## 3.3. Crystallite Size Characterisation

The final crystallite size was determined by optical image analysis using a Malvern Morphologi G3<sup>42</sup>. Crystal samples were obtained from the sample vials after the

crystallisation experiments at a supersaturation of 1.2, by isolating the solids from solution using vacuum filtration. These crystals were then dried in an oven at 50°C. The samples of crystals were manually dispersed onto the automated glass sample stage with a spatula to prevent crystallite breakage. The imaging program scanned a predetermined circular area of sample using a 20x magnification lens providing resolution of 3.5 - 210  $\mu\text{m}$ . Light intensity and lens focus were automatically calibrated using the instrument software from each measurement. The size distributions provided from this analysis were  $d_{0.1}$ ,  $d_{0.5}$  and  $d_{0.9}$ .

### **3.4. Solvation free energies of PABA using molecular dynamics**

The solvation free energies of PABA were predicted with molecular dynamics simulations using the thermodynamic integration technique<sup>43</sup>. Each of the states of PABA sampled was first minimised using the steepest descents method<sup>44</sup>. Then each state was equilibrated at 293 K and 1 atm for 100 ps. The initial state ( $\lambda=0$ ) was defined by turning off the electrostatic and VDW interactions between the solute and the solvent. The final state ( $\lambda=1$ ) was defined as having the single molecule fully solvated in a solvent box. Eight ‘windows’ were used for the integration pathway going from the initial to the final state  $\Delta\lambda= 0.0\ 0.2\ 0.4\ 0.6\ 0.7\ 0.8\ 0.9\ 1.0$ . For each window, further equilibration of the system was applied for 100 ps and sampled for 500 ps. All calculations are performed within the Gromacs programs package<sup>45</sup>. Topology files, bonded and non-bonded parameters were derived from the GAFF force field<sup>46</sup>. For the electrostatic potential, RESP charges were derived from Antechamber<sup>47</sup> within Ambertools based on ab-initio calculations at the MP2/aug-cc-pvTz level of theory.

## 4. Results and Discussion

This section provides detailed analysis of the crystallisation behaviour of PABA, drawing together data and analysis regarding solubility characterisation (section 4.1), meta-stable zone-width determination (section 4.2), nucleation kinetics and mechanism (section 4.3) and crystal growth mechanism (section 4.4). The above work is integrated (section 4.5) through relating the crystallisability of PABA to crystallisation solvent type and solute concentration.

### 4.1. Solubility, Solution Thermodynamics

The solubility, solution thermodynamics and meta-stability of PABA were assessed for the three solvents. An example of cooling and turbidity profiles for crystallisation from water is shown in Figure 3a) and b), highlighting the determination of  $T_e$  as a function of solution concentration and solvent from the extrapolation of the values for  $T_{dis}$  and  $T_C$ . The van't Hoff plots of the solubility for PABA in ethanol, acetonitrile and water solutions, shown in Figure 3c), d) and e) were consistent with less than ideal behaviour indicating a preference for solute – solute interactions in all three solvents. In terms of the closest to solution ideality the order was ethanol > acetonitrile > water which is consistent with the relative solubility of PABA and with an inverse relationship to the dielectric constants of these solvents<sup>48</sup>.

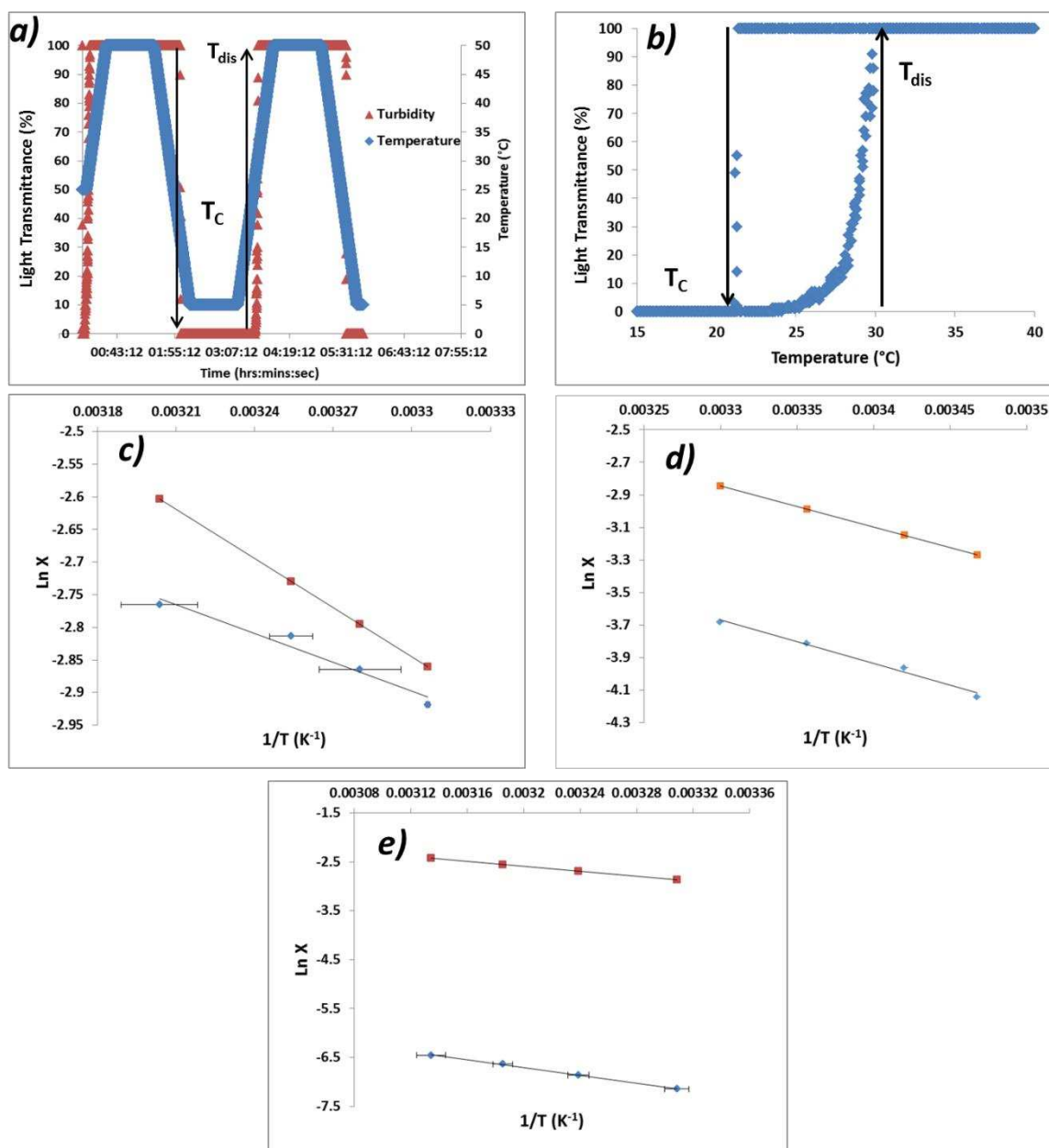


Figure 3: a) Typical poly-thermal cooling crystallisation profile from water, highlighting turbidity measurements (light transmittance %) of  $T_{dis}$  and  $T_C$ , b) light transmittance % vs temperature indicating extrapolation of  $T_{dis}$  and  $T_C$ , c) *van't Hoff plot of the solubility measured from poly-thermal analysis vs the ideal solubility in ethanol*, d) *in acetonitrile* and e) *in water solutions*

The calculated activity coefficients,  $\gamma$ , together with the values of the enthalpy and entropy of dissolution at solution saturation,  $\Delta H_{diss}$  and  $\Delta S_{diss}$ , are given in Table 1. The lowest values of  $\Delta H_{diss}$  and  $\Delta S_{diss}$  are calculated for ethanol, and the highest for water while the values for



acetonitrile lie between the two. As these values are calculated at saturation concentration this trend mirrors the measured solubility and indicate that the dissolution process is driven by the enthalpy change, this was also highlighted from the calculated free energy term,  $\Delta G_{\text{diss}}$ .

Table 1: *Calculated values for the activity coefficient,  $\gamma$ , enthalpy of dissolution  $\Delta H_{\text{diss}}$ , entropy of dissolution  $\Delta S_{\text{diss}}$ , free energy of dissolution  $\Delta G_{\text{diss}}$  and enthalpy of solvation  $\Delta H_{\text{solv}}$  for each solvent from a van't Hoff analysis (assuming negligible changes of  $\Delta C_p$  with temperature) of the measured concentration values from poly-thermal analysis and the MD simulation results of solvation free energy calculated for a monomer of PABA in ethanol, acetonitrile and water solutions respectively*

Solvent	$\gamma$	$\Delta H_{\text{diss}}$ (kJ/mol)	$\Delta S_{\text{diss}}$ (kJ/ K <sup>-1</sup> mol <sup>-1</sup> )	$\Delta G_{\text{diss}}$ (kJ/mol)	$\Delta H_{\text{solv}}$ (kJ/mol)	$\Delta G_{\text{solv}}$ from MD higher concentration (kJ/mol)	$\Delta G_{\text{solv}}$ from MD lower concentration (kJ/mol)
Ethanol	1.10	12.3	0.017	7.2	-95.4	26.40 g/kg = - 58.5 +/-1.7	18.87 g/kg = - 53.5 +/-1.6
Acetonitrile	2.31	22.3	0.043	9.6	-85.3	63.96 g/kg = - 54.5 +/-0.9	29.86 g/kg = - 52.9 +/-1.0
Water	63.05	33.3	0.051	17.5	-74.4	22.7 g/kg = - 42.4 +/-1.2	10.79 g/kg = - 43.9 +/-1.7

The calculated values of  $\Delta H_{\text{solv}}$  shown in Table 1 indicate that at saturation, the solvation enthalpy in ethanol is -95.4 kJ/mol and -74.4 kJ/mol in water; this can also be interpreted as the energy required to de-solvate a molecule of PABA at saturation concentration. This trend was further supported by the calculated values of free energy of solvation,  $\Delta G_{\text{solv}}$ , from MD simulations at two concentrations, presented in Table 1.  $\Delta G_{\text{solv}}$  at the lower concentration in ethanol was found to be -53.5 kJ/mol and -43.9 kJ/mol in water, and hence de-solvation of PABA in the three solvents is most energetically favourable in water followed by acetonitrile and least favourable in ethanol. At the higher concentration this trend remains the same, however,  $\Delta G_{\text{solv}}$  was calculated as -58.5 kJ/mol in ethanol indicating an increase of solution

concentration resulted in a larger increase in the de-solvation energy compared to water. The  $\Delta G_{\text{solv}}$  in water at higher concentrations was calculated as -42.4 kJ/mol, which indicated de-solvation in water is energetically more favourable with increasing solution concentration.

#### 4.2. Determination of meta-stable zone-width

The meta-stable zone-width for PABA was assessed by analysis of the  $T_{\text{dis}}$  and  $T_{\text{C}}$  values as a function of cooling rate to calculate  $\Delta T_{\text{c}}$ ; an example of calculated  $\Delta T_{\text{c}}$  values for solutions in ethanol, acetonitrile and water is presented in Table 2 with example data provided in Figure 4. The full list of dissolution and crystallisation temperatures together with calculated  $\Delta T_{\text{c}}$  values for all cooling rates in ethanol, acetonitrile and water can be found in the supplementary material.

Table 2: *Calculated  $\Delta T_{\text{c}}$  values from analysis of the crystallisation and dissolution temperatures in 170g/kg ethanol, 54 g/kg acetonitrile and 6 g/kg water solutions*

Cooling Rate ( $^{\circ}\text{C}/\text{min}^{-1}$ )	$\Delta T_{\text{c}}$ Ethanol / $^{\circ}\text{C}$	$\Delta T_{\text{c}}$ Acetonitrile / $^{\circ}\text{C}$	$\Delta T_{\text{c}}$ Water / $^{\circ}\text{C}$
0.1	6.9(1)	6.8(1)	6.5(6)
0.3	13.2(1)	9.1(8)	8.1(4)
0.5	21.4(6)	8.2(6)	8.6(6)
0.7	23.9(1)	10.1(0)	8.0(6)
1	29.9(8)	10.0(0)	10.5(8)

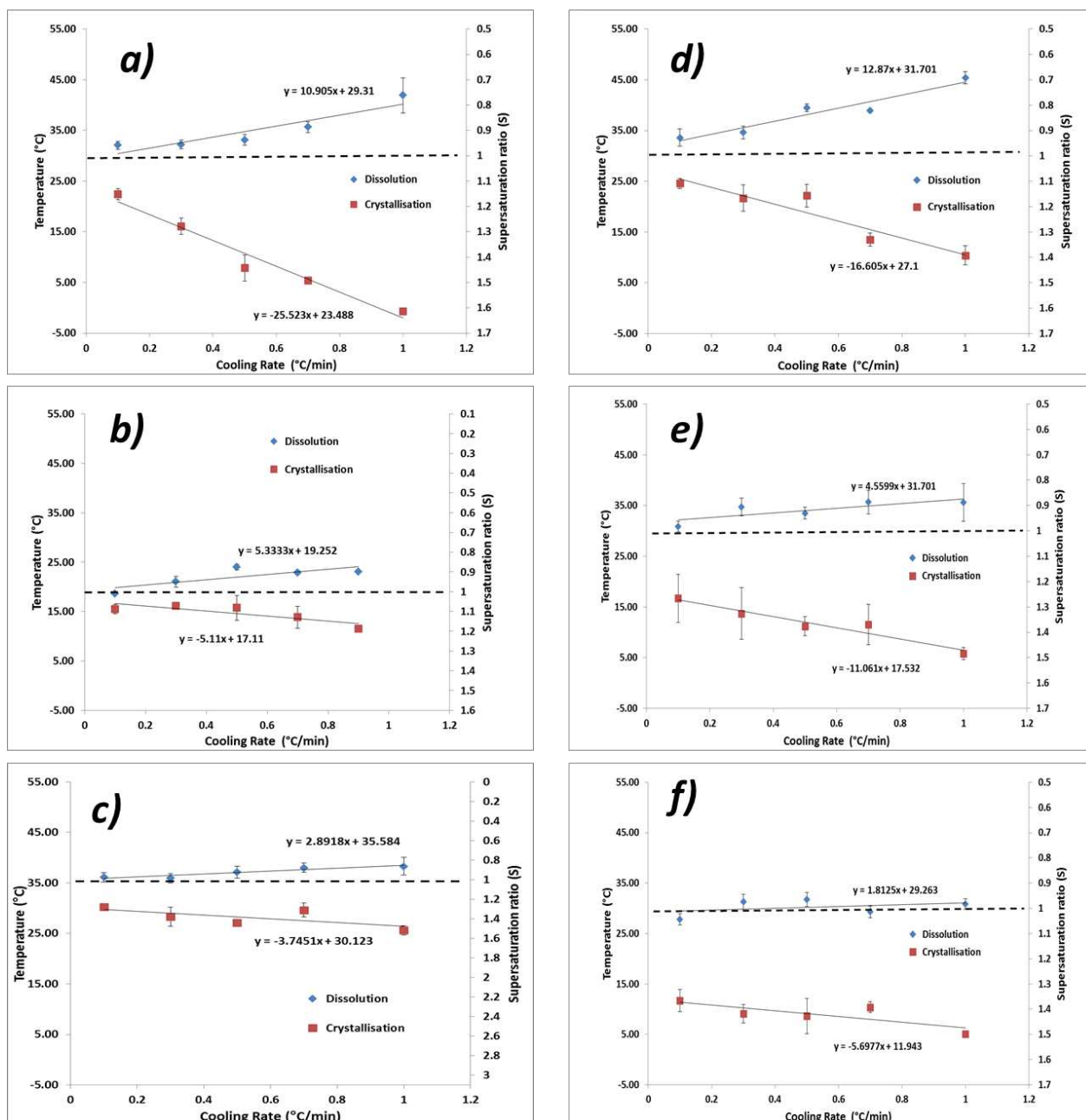


Figure 4:  $T_{dis}$ ,  $T_C$  and supersaturation ratio as a function of cooling rate recorded for a solution concentration of a) 170 g/kg in ethanol, b) 54g/kg in acetonitrile, c) 8g/kg in water, d) 180g/kg in ethanol, e) 160 g/kg in ethanol and f) 150 g/kg in ethanol.

These data, which highlight the dependence of crystallisation and dissolution temperature on solution cooling rate, show a high dependence on cooling / heating rates for both the crystallisation and dissolution on-set points for crystallisation in ethanolic solutions (Figure 4a). This suggests that the crystallisation process was rate limited by nucleation rather than by supersaturation generation due to cooling. To a lesser extent acetonitrile solutions (Figure 4b) were also found to exhibit a small dependence of their crystallisation and dissolution on-set points on cooling rate whereas, in contrast, the related data for water solutions (Figure 4c) exhibited little variation with cooling rate. The latter indicated that beyond a critical supersaturation of ca 1.1, the solutions can nucleate comparatively easily and hence significant solution super-cooling beyond this threshold is not observed. This trend was also observed for ethanolic PABA solutions for lower solute concentrations, as highlighted in Figure 4d), e) and f), where the crystallisation temperatures were found to exhibit less dependence on cooling rate with decreasing concentration. A full set of plots of super-solubility and solubility curves, as derived from extrapolation of  $T_e$  and  $T_c$  at  $0^\circ\text{C}/\text{min}$  cooling rate for the three solvents are provided in the supplementary material.

### **4.3. Analysis of the Nucleation Kinetics and Mechanism**

Polythermal data analysis of  $\ln u_c$  vs  $\ln q$ , for ethanol, acetonitrile and water solutions at solute concentrations of 170, 54 and 6 g/kg respectively are given in Figure 5 a), b) and c) with the results of the KBHR analysis being given in Table 3. Examination of the data from the ‘rule of three’ analysis reveals that for all solute concentrations studied in ethanoic solutions, with the exception of the 160 and 150 g/kg solutions, the slope of these plots is  $< 3$ , revealing the nucleation mechanism in the higher concentration range studied to be instantaneous. In contrast for the two lower concentrations the nucleation mechanism was found to be progressive.

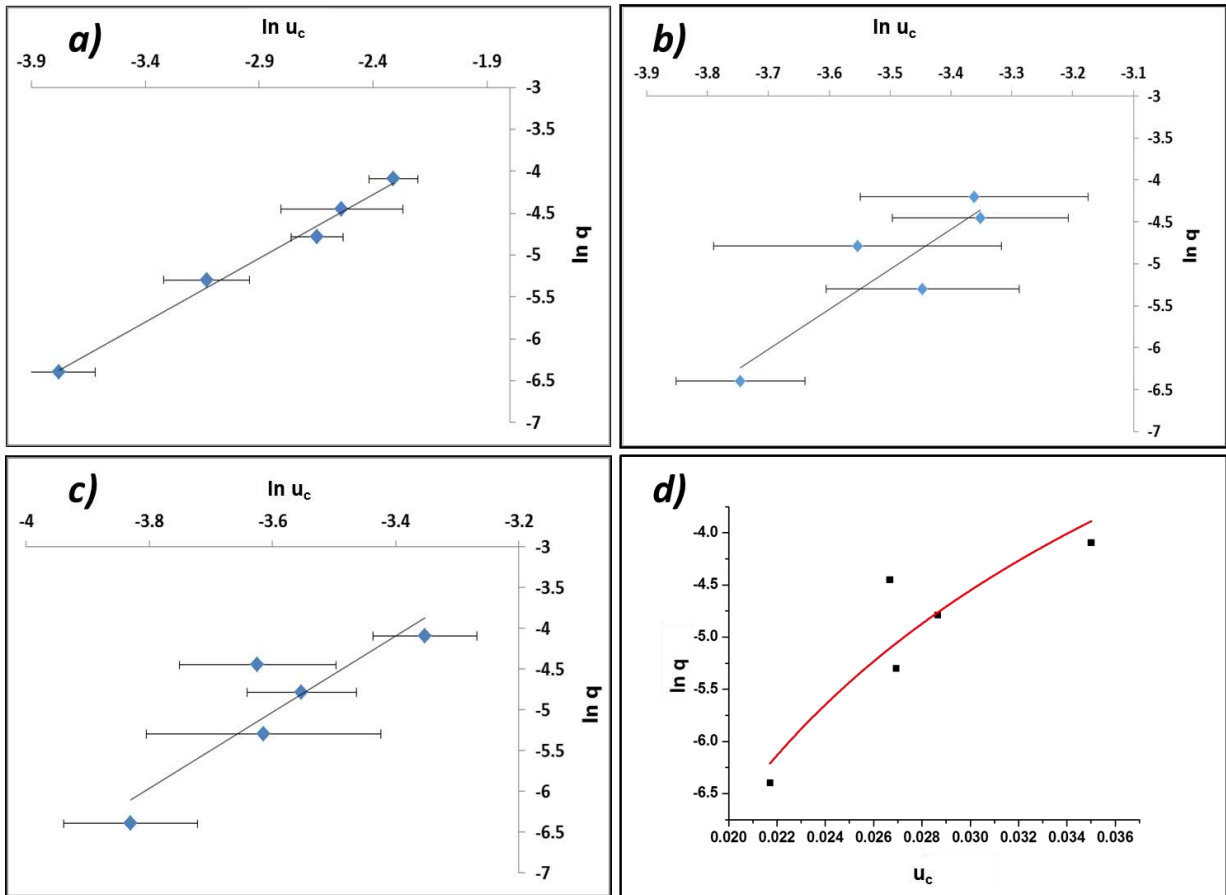


Figure 5: a) plot of  $q$  vs  $\mu c$  in  $\ln$ - $\ln$  coordinates for PABA in ethanol at a concentration of 170 g/kg b) in acetonitrile at a concentration of 54 g/kg c) in water at a concentration of 6 g/kg d) Relative critical undercooling as a function of  $\ln$  cooling rate for a solution concentration of 6 g/kg in water, highlighted is the results of the best fit of Equation 10 to the data

These results were mirrored in the analysis of the acetonitrile solutions with the higher concentrations being consistent with instantaneous nucleation, with the lower solute solution concentration data at 54 g/kg revealing a much larger slope of 3.21 consistent with a progressive nucleation mechanism. Similarly, the results in higher concentration water solutions also reveal an instantaneous nucleation mechanism with a progressive mechanism for the lower concentration values e.g. 6 g/kg.

The slopes of these regressions in water however, were found to be much closer to 3 i.e. that required for progressive nucleation, thus indicating that in water, PABA nucleates more readily. Conversely in ethanol and acetonitrile, putative nuclei seem to be stable for longer

time periods which is consistent with the larger undercoolings observed for these solvents. Interestingly the ethanolic PABA solutions highlight a concentration dependence upon the nucleation mechanism of the system whereby a change of mechanism from instantaneous to progressive occurs with decreasing concentration within a critical range from 170 to 160 g/kg.

The error bars highlighted in the  $\ln q$  vs  $\ln u_c$  plots in Figure 5 highlight the stochastic nature of crystallisation, where the recorded values of  $T_c$  provide a variation in the MSZW and hence  $u_c$ . It should be noted that the derived  $T_c$  and  $T_{dis}$  values were the average of between 5-8 experimental repetitions which complies with the guidance of the comprehensive error analysis of the KBHR method provided in CrystEngComm, 2014, 16, 974 supplementary material<sup>25</sup>.

Table 3: Calculated nucleation kinetics as a function of concentration for alpha PABA in ethanol, acetonitrile and water from the slope and intercept of the linear fit to  $q$  vs  $u_c$  in ln-ln coordinates

Conc. (g/kg)	$T_e$ (°K)	Slope of ln $q$ vs. ln $u_c$	$R^2$ of linear fit to ln $q$ vs ln $u_c$	Nucleation mechanism	$q_0$ (K s <sup>-1</sup> )	$n$	$\gamma_{\text{eff}}$ (mJ/m <sup>2</sup> )	$C_0$ (m <sup>-3</sup> )	Nuclei/1 ml	$r^*$ (nm)	$\Delta T_c$ range °C
<b>Ethanol</b>											
150	302.4(1)	3.69	0.64	Progressive	N/A	N/A	2.71 <sup>†</sup>	1.83×10 <sup>10</sup>	N/A	0.30 – 0.49	16.1(0) – 25.7(8)
160	304.8(5)	3.25	0.97	Progressive	N/A	N/A	1.79 <sup>†</sup>	1.33×10 <sup>10</sup>	N/A	0.17 - 0.37	14.2(0) – 29.8(0)
170	302.4(6)	1.68	0.99	Instantaneous	1.36	0.68	N/A	8.60×10 <sup>8</sup>	860	N/A	8.3(0) – 31.3(7)
180	304.8(5)	1.76	0.80	Instantaneous	1.86	0.76	0.85 <sup>‡</sup>	1.18×10 <sup>9</sup>	1180	0.69–1.98	7.3(2) – 21.5(0)
190	307.3(2)	1.56	0.53	Instantaneous	1.65	0.56	N/A	1.06×10 <sup>9</sup>	1057	N/A	5.6(3) – 17.1(0)
200	312.1(3)	1.62	0.62	Instantaneous	3.1	0.62	1.31 <sup>‡</sup>	1.96×10 <sup>9</sup>	1957	0.48–0.91	4.2(2) – 13.8(5)
<b>Acetonitrile</b>											
54.0	288.4(2)	4.77	0.8	Progressive	N/A	N/A	1.13	3.22×10 <sup>13</sup>	N/A	0.53 - 0.84	6.8(1) – 10.0(0)
64.8	292.4(5)	1.56	0.43	Instantaneous	4.53	0.56	N/A	2.84×10 <sup>9</sup>	2838	N/A	3.7(8) – 7.7(5)
75.6	297.9(8)	1.61	0.34	Instantaneous	8.58	0.61	N/A	5.36E×10 <sup>9</sup>	5364	N/A	2.9(6) – 4.8(5)
86.4	303.1(1)	1.99	0.96	Instantaneous	38.86	0.99	N/A	2.42×10 <sup>10</sup>	24221	N/A	2.1(9) – 5.5(1)
<b>Water</b>											
6	302.2(5)	4.53	0.79	Progressive	N/A	N/A	1.95	3.45×10 <sup>11</sup>	N/A	0.53 - 0.84	6.5(6) – 10.5(8)
8	308.7(5)	2.41	0.49	Instantaneous	54.60	1.41	N/A	2.18×10 <sup>10</sup>	21805	N/A	5.3(8) – 9.9(8)
10	313.9(5)	2.39	0.62	Instantaneous	94.63	1.39	N/A	3.78×10 <sup>10</sup>	37814	N/A	3.5(2) – 7.1(8)
12	319.0(5)	2.13	0.95	Instantaneous	44.70	1.13	N/A	1.78×10 <sup>10</sup>	17836	N/A	2.6(0) – 6.2(4)

<sup>†</sup>calculated from poly-thermal KBHR analysis, <sup>‡</sup>calculated from iso-thermal analysis referenced in Toroz et al<sup>34</sup>

The values calculated for  $C_0$  at the various solution concentrations are presented in Table 3, the values show good agreement with calculated values for aspirin, a similar organic molecule, using this methodology.<sup>49</sup> The relevant values of nuclei/ml for the three solvents were found, in general, to be low for ethanol solutions and higher for acetonitrile and water. This observed trend follows an inverse relationship to solubility; PABA has the highest solubility in ethanol (144.0 g/kg at 20°C), but is found to nucleate the lowest number of nuclei at  $T_0$ , whereas in water the solubility of PABA is very low (3.4 g/kg at 20°C), however a large number of nuclei are formed upon instantaneous nucleation.

The data measured at lower concentrations of the ethanol acetonitrile and water solutions, which displayed progressive nucleation behaviour, were further analysed using Equations 10-15. An example of this curve fitting for a water solution at a concentration of 6g/kg is highlighted in Figure 5d). The results of the fitting procedure were correlated to  $\gamma_{\text{eff}}$  for each solvent and concentration which displayed a progressive nucleation mechanism through Equation 12. Table 3 contains the values of  $r^*$  and  $i^*$  from Equations 14 and 15, this was calculated for the high and low values of critical undercooling; 0.047 – 0.098 in ethanol, 0.024 – 0.035 in acetonitrile and 0.022 – 0.035 in water.

The results from the progressive nucleation analysis seem to indicate that the interfacial tension values for all three solvents were relatively low. The values in acetonitrile were found to be in reasonable agreement with calculated literature values of  $\gamma_{\text{eff}}$  for PABA solutions in acetonitrile from induction time measurements, where a value of 1.33 mJ/m<sup>2</sup> was presented<sup>7</sup>. Further literature values of  $\gamma_{\text{eff}}$  calculated from induction time analysis in higher concentration ethanolic PABA solutions, were found to be 0.85 and 1.31 mJ / m<sup>2</sup> for concentrations of 180 g/kg and 200 g/kg respectively. Comparatively the calculated values of  $\gamma_{\text{eff}}$  from the KBHR analysis are also relatively low for the lower concentration ethanolic PABA solutions, where



values of 1.79 and 2.71 mJ/m<sup>2</sup> were calculated at concentrations of 160 and 150 g/kg respectively.

#### **4.4. Analysis of the Mechanism for Crystal Growth**

The results of the KBHR analysis were utilised to explain the crystal growth of PABA in the three solvents and this was further supported by experimental measurement of the recovered crystallite sizes. The value of the growth exponent, *n*, highlighted in Table 3 for ethanol and acetonitrile solutions was found to be 1, on average this value was slightly higher in acetonitrile. This is indicative of a system where the growth of the crystallites is rate limited only by mass transfer i.e. the diffusion of the growth unit to the growing crystallite. The results in water however have revealed that the average value of *n* is much closer to 2 and as such this is indicative of a system whereby growth is rate limited by rearrangement of the solute at the crystal/solution interface. Further to this, it was observed that the size of the crystallites recovered from the polythermal crystallisations varied between the three solvent systems. Micrographs of the recovered crystallites indicated that the crystals recovered from ethanol and acetonitrile were generally significantly larger than those recovered from water, this comparison is provided in Figure 6(a), b) and c).

Results from the optical image analysis of crystallite size in Figure 6(d) shows the crystallite length distributions for the crystals recovered from crystallisation experiments. The length distribution mean values in Table 4 were found to be 37.25 μm in water compared to 90.64 μm in acetonitrile and 113.11 μm in ethanol, this was further supported by the recorded values of length distributions; *d*<sub>0.1</sub>, *d*<sub>0.5</sub> and *d*<sub>0.9</sub>. For example, the crystallite length *d*<sub>0.9</sub> in ethanol is considerably larger, 262.90 μm, when compared to the same distribution in water at 92.60 μm.

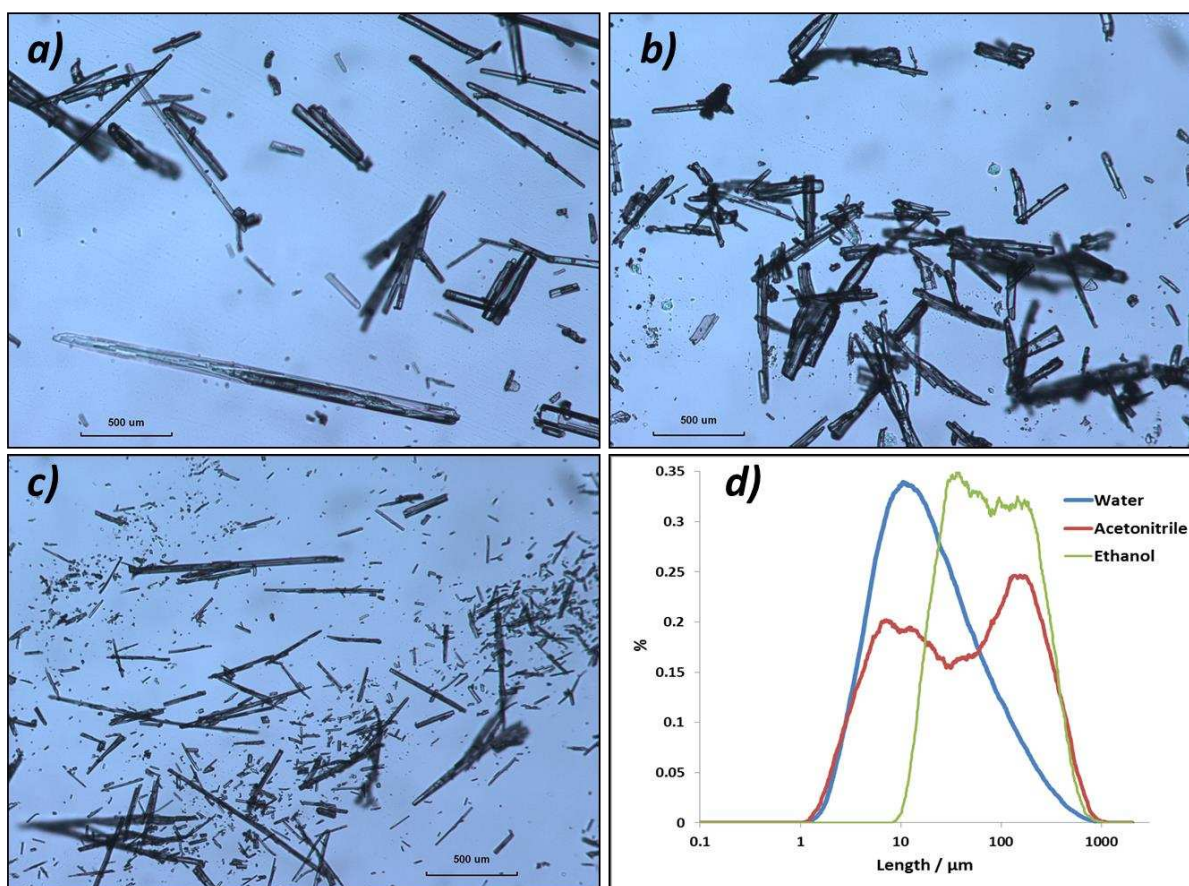


Figure 6: micrographs of crystals recovered from poly-thermal cooling experiments from a) ethanol, b) acetonitrile c) water solutions d) length distributions of recovered crystallites from cooling crystallisations at supersaturations = 1.2 using optical analysis.

Table 4: Results of optical analysis of crystallites recovered from cooling crystallisations in ethanol, water and acetonitrile, highlighting the measured crystallite length distributions and width distributions

<b>Solvent</b>	<b>Mean Length <math>\mu\text{m}</math></b>	<b>Length <math>\mu\text{m}</math> d0.1</b>	<b>Length <math>\mu\text{m}</math> d0.5</b>	<b>Length <math>\mu\text{m}</math> d0.9</b>
Ethanol	113.11	23.26	72.94	262.90
Acetonitrile	90.64	4.60	40.01	247.63
Water	37.25	4.98	14.89	92.60
<b>Solvent</b>	<b>Mean Width <math>\mu\text{m}</math></b>	<b>Width <math>\mu\text{m}</math> d0.1</b>	<b>Width <math>\mu\text{m}</math> d0.5</b>	<b>Width <math>\mu\text{m}</math> d0.9</b>
Ethanol	23.13	7.15	16.64	45.91
Acetonitrile	21.39	2.54	11.91	51.08
Water	9.06	2.26	5.06	17.27

The crystallite width distribution analysis highlighted in Table 4, affords quantitative support of the observation that crystallites recovered from acetonitrile and ethanol were generally wider than those that are grown in water. This can also be seen in the micrographs in Figure 6 which indicates that the crystals recovered from ethanol were generally longer along the needle axis and their crystallographic surfaces were more clearly defined, particularly when compared to crystals grown in water. The crystallites recovered from acetonitrile are generally crystallographically well-defined and were also found to be wider than the crystals recovered from water which usually exhibited shorter needle-like crystals with much less defined facets. It should be noted that whilst the trend in crystal size between these three solvents is clear, some caution should be exercised in terms of over interpreting this size data mindful of the potential of inter-particle attrition within the crystallisation vessel.

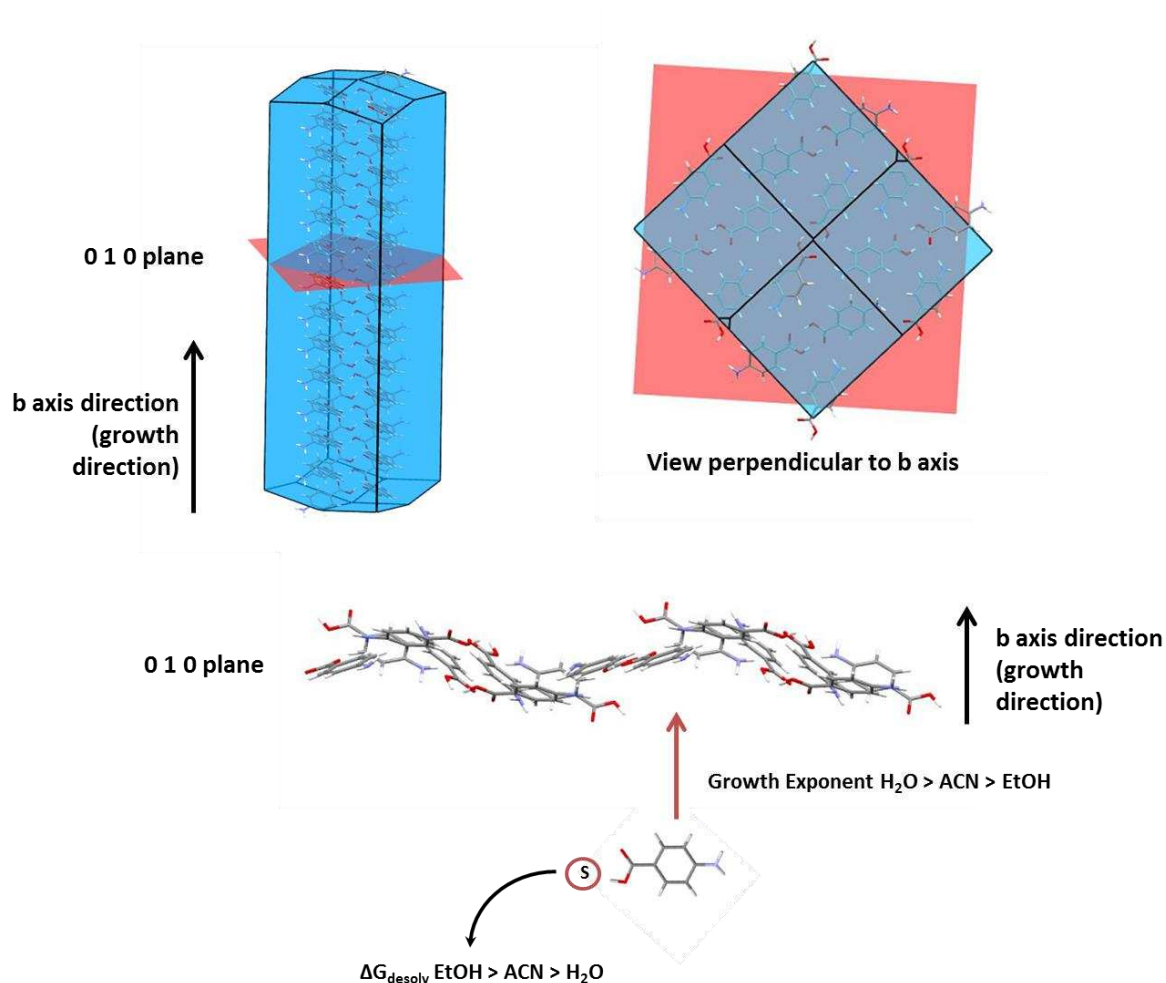


Figure 7: An illustrated example of the possible pathway to nucleation and growth of alpha PABA considering addition to the fastest growing (0 1 0) plane of the needle b axis

<sup>50</sup>Further to this, Rosbottom et al<sup>Error! Bookmark not defined.</sup> have recently concluded that the growth direction of PABA crystals is found to be along the b axis in the (0 1 0) plane, where the fast growing needle axis is dominated by  $\pi$ - $\pi$  stacking interactions of the aromatic rings. Considering  $n = 1$  in ethanol and acetonitrile solutions and 2 in water solutions, if the only barrier to crystal growth were the free energy of de-solvation, it should be expected that crystals would be largest in water where the growth unit can de-solvate at a greater rate. However, the trend is the contrary and so it is likely that the attachment frequency to the fast growing (0 1 0) plane is relative to crystallite size. This suggests that there is a barrier to growth at the (0 1 0) surface in water which is not present or is decreased to a large extent in ethanol and acetonitrile solutions. Sullivan et al<sup>7</sup> have recently indicated the importance of dimer formation as a key step in attachment to the PABA crystal during crystallisation. Additionally, Toroz et al<sup>34</sup> have suggested that COOH dimer formation may occur in supersaturated solutions of PABA in ethanol; this leads to speculation that formation of the COOH dimer could be the rate limiting step for growth allowing a favourable  $\pi$ - $\pi$  stacking interaction to occur at the (0 1 0) plane. This mechanism for growth is presented in Figure 7, where the de-solvation process takes place before addition to the fast growing (0 1 0) plane.

#### **4.5. Crystallisability in Relation to Solution Chemistry**

The data reported in this work are summarised in Table 5 and can be applied in order to gain an improved understanding of the role played by solvent in the self-assembly, nucleation and ultimately crystal growth of PABA from the various solvents studied. The values of  $\Delta H_{\text{solv}}$  calculated in the van't Hoff analysis follow the same trend as those calculated from MD simulations, -74 kJ/mol in water solutions and -95 kJ/mol in ethanol, where de-solvation of PABA in water costs less free energy in comparison to the case in ethanol. This trend also seems to correlate well with the molecular structure of the solvent and its ability to solvate

PABA, where water poorly solvates PABA and hence the energetic penalty for de-solvation is less than the case of ethanol, which solvates PABA strongly.

The free energy of de-solvation is an important factor when considering the nucleation rate of a solute and therefore is directly related to the achievable undercooling of a solution prior to crystallisation. The values of  $\Delta H_{\text{solv}}$  directly correlate with the measured values of  $u_c$ , whereby undercooling was greatest in ethanol and de-solvation is expected to be slowest, conversely in water the calculated values of  $u_c$  are less than those in ethanol and de-solvation is expected to be faster. Recent work relating attachment frequency,  $f^*$ , to the free energy of de-solvation of PABA by Sullivan et al <sup>7</sup> has shown that  $f^*$  increases with decreasing de-solvation free energy of the carboxylic acid group. So it might be expected that the rate of nucleation is strongly proportional to the de-solvation free energy of the solute in a saturated solution. This leads to the postulation that the nucleation rate in general is likely to be lower in ethanol than in water at relevant supersaturation and temperature, in line with the calculated values of  $\Delta H_{\text{solv}}$  and  $\Delta G_{\text{solv}}$  from van't Hoff analysis and MD simulation respectively.

The calculated values of interfacial tension,  $\gamma_{\text{eff}}$ , from the progressive nucleation analysis at the lower concentration of 6g/kg in water solutions were found to be 1.95 mJ/m<sup>3</sup>, this is significantly higher than the values of  $\gamma_{\text{eff}}$  calculated in ethanol which were found to be 0.85 – 1.31 mJ/m<sup>2</sup> by Toroz et al. According to classical theory the nucleation rate  $J(t)$  is given by

$$J(t) = K_J e^{\frac{-b}{(1-u)u^2}} \quad \text{(Equation 16)}$$

where  $b$  is the thermodynamic exponential function which is related to the interfacial tension,  $\gamma_{\text{eff}}$  through Equation 17;

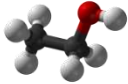
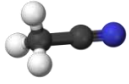
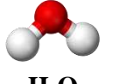
$$b = \frac{k_n v_0^2 \gamma_{\text{eff}}^3}{kT e \lambda^2} \quad \text{(Equation 17)}$$

and where the nucleation rate constant  $K_J$  is related to the Zeldovich factor,  $z$ ,  $C_0$  and the frequency of attachment of the molecular building blocks to the nucleus,  $f^*$  <sup>25,38</sup>.

$$K_J = z f^* C_0 \quad (\text{Equation 18})$$

Considering this, an argument can be made that in the case of ethanolic PABA solutions  $J_{(t)}$  is not limited by the  $\gamma_{\text{eff}}$  and hence the thermodynamic parameter  $b$ , but is instead limited by  $f^*$ , which is likely a consequence of a higher free energy of de-solvation. This is also supported by the observed kinetic dependence of  $T_{\text{dis}}$  and  $T_C$  on cooling rate highlighted in Figure 4a), b) and c). Comparatively the case in water can be expected to be the contrary situation where now  $J_{(t)}$  is likely to be limited by  $\gamma_{\text{eff}}$  and not by  $f^*$ , this is again consistent with the observation of the lesser cooling-rate dependant crystallisation parameters whereby the dependence of  $T_{\text{dis}}$  and  $T_C$  on cooling rate is not significant.

Table 5: Solvent properties and a summary of results from van't Hoff, solution thermodynamics and KBHR analysis of the poly-thermal data collected

	<b>Ethanol</b>  <b>CH<sub>3</sub>CH<sub>2</sub>OH</b>	<b>Acetonitrile</b>  <b>CH<sub>3</sub>CN</b>	<b>Water</b>  <b>H<sub>2</sub>O</b>
<b>Dielectric Constant</b>	24.3	37	78
<b># Atoms</b>	9	6	3
<b>Solubility at 20°C / g/kg</b>	144.4	65	3.41
<b>Solution Ideality</b>	Most ideal case		Least ideal case
<b>Activity Coefficient <math>\gamma</math></b>	1.10	2.31	63.05
<b><math>\Delta H_{\text{solv}}</math> / kJ/mol (from experimental solubility measurements)</b>	-95.4	-85.3	-74.4
<b><math>\Delta G_{\text{solv}}</math> / kJ/mol (from MD simulation)</b>	-53.5	-52.0	-41.0
<b>Cooling effect on <math>T_{\text{dis}}</math> and <math>T_{\text{c}}</math></b>	Kinetic	Kinetic	Thermodynamic
<b>Degree of solution undercooling</b>	High	Low	Low
<b><math>C_0</math> Nuclei concentration / m<sup>-3</sup></b>	$8.60 \times 10^8 - 1.96 \times 10^9$	$2.84 \times 10^9 - 2.42 \times 10^{10}$	$1.78 \times 10^{10} - 3.78 \times 10^{10}$
<b>Growth exponent <math>n</math></b>	0.56-0.76	0.56-0.99	1.13-1.41
<b>Growth rate limiting, from <math>n</math></b>	Mass Transport	Mass Transport	Interface Kinetics
<b>Mean Crystallite Length / <math>\mu\text{m}</math></b>	113.11	90.64	37.25

Further to this, an interesting cross-correlation was made between the calculated values of the  $C_0$ ,  $\Delta H_{\text{solv}}$  and  $\Delta G_{\text{solv}}$ . The values of  $C_0$  in ethanol were found to be  $8.60 \times 10^8 - 1.96 \times 10^9 \text{ m}^{-3}$  which is much lower than the case in water with values of  $1.78 \times 10^{10} - 3.78 \times 10^{10} \text{ m}^{-3}$ . However, considering that  $\Delta H_{\text{solv}}$  and  $\Delta G_{\text{solv}}$  are greatest in water, thus de-solvation is likely to be more favourable, and  $f^*$  is likely lower in comparison to ethanol, this further supports the conclusion that nucleation rates would be higher in water as consistent with the observed

lower values of  $\mu_c$ . The case of acetonitrile solutions seems to lie within the middle of the water and ethanol solutions in terms of the values of  $\Delta H_{\text{solv}}$  and  $\Delta G_{\text{solv}}$  and as such the nucleation rate will likely be a middle value between the two. These results and observations are consistent with an inter-molecular association model for the crystallisation of PABA, whereby water fails to stabilise the non-polar moieties of the PABA molecule in solution which leads to lower free energy of de-solvation resulting in a higher nucleation rate. Similarly nuclei are not stabilised by the polar water molecules resulting in a lower barrier to nucleation and hence lower  $\mu_c$  values. The opposite case can be expected for ethanol where a larger free energy of de-solvation, due to stabilisation of the non-polar benzene ring, affords a higher degree of undercooling. It should be noted that although the results of this analysis give a good indication of the nucleation behaviour at the molecular scale for PABA, the exact structure and size of the nuclei discussed have yet to be determined and future studies are required.



## 5. Conclusions

The paper highlights the importance of considering the chemical properties of a solvent in influencing and directing the de-solvation process, nucleation mechanism and hence growth kinetics of a crystallisation system. It has been demonstrated that ethanol can stabilise the supersaturated state of PABA during nucleation, acetonitrile offers less stabilisation compared to ethanol whilst water appeared to provide very little stabilisation at all which is reflected in the calculated values of  $u_c$ . This trend is also seen in the thermodynamics of de-solvation; where the magnitude of  $\Delta G_{\text{solv}}$  was found to follow the trend water > acetonitrile > ethanol.

The nucleation mechanism was found to be instantaneous at higher concentrations and progressive at lower concentrations in all solvents. The concentration effect which increased the progressive nature of nucleation with decreasing concentration was found to be associated with an increase in attachment frequency,  $f^*$ , combined with a higher value for the interfacial tension,  $\gamma_{\text{eff}}$ , at the lower concentrations causing the thermodynamic component of the nucleation rate to become rate limiting. This resulted in a more thermodynamically controlled process and hence a more progressive mechanism.

The nuclei concentration upon instantaneous nucleation followed the trend water > acetonitrile > ethanol. The calculated interfacial tensions at the lower concentrations in water and acetonitrile solutions were found to be 1.95 and 1.13 mJ/m<sup>3</sup> respectively. The growth exponent,  $n$ , followed the trend of water solutions > acetonitrile > ethanol suggesting that there is a barrier to growth in water solutions at the surface of the growing crystallite which is not apparent, or relatively decreased, in the cases of ethanol or acetonitrile. This was extended to the habit surfaces important in the growth along the needle axis. This was found

to correlate well with measured crystallite lengths in ethanol, acetonitrile and water solutions were crystals recovered from ethanol and acetonitrile were found to be longer along the needle axis than those recovered from water solutions.

Overall this work highlights the value of the poly-thermal technique in terms of providing a fully integrated analysis of a crystallisation process. The latter is assessed as a function of cooling rate, solute concentration and solvent choice, through a study encompassing both experimental studies and computational molecular modelling.

### **Acknowledgements**

The authors gratefully acknowledge the UK's Engineering and Physical Sciences Research Council for the funding of this research through a joint collaborative Critical Mass project between the Universities of Leeds and Manchester (grant references EP/IO14446/1 and EP/IO13563/1) which forms part of the doctoral studies of TDT. One of us (DMCC) gratefully acknowledges Infinium UK for the funding of a PhD studentship. We also gratefully acknowledge the Critical Mass team at the University of Manchester for stimulating discussions which contributed to the research presented in this paper. The development of the KBHR method was facilitated through a Leverhulme visiting Professorship grant awarded to Professor Dimo Kashchiev who we gratefully acknowledge and thank.

## List of Symbols

$A_0$	Fixed needle cross sectional area ( $\text{m}^2$ )
$a$	Dimensionless molecular latent heat of crystallisation
$\alpha$	activity
$\alpha_{\text{det}}$	Detectable fraction of crystallised volume
$b$	Dimensionless thermodynamic parameter
$C_e$	Equilibrium solution concentration ( $\text{m}^{-3}$ )
$C_0$	Concentration of instantaneously nucleated crystallites ( $\text{m}^{-3}$ )
$C_p$	Specific heat capacity ( $\text{J/kg.K}$ )
$d$	Dimensionality of crystallite growth
$E_{\text{latt}}$	Lattice energy ( $\text{KJ/mol}$ )
$f^*$	Attachment frequency
$\Delta G_{\text{solv}}$	Free energy of solvation ( $\text{KJ/mol}$ )
$\Delta G_{\text{diss}}$	Free energy of dissolution ( $\text{KJ/mol}$ )
$\Delta H_{\text{fus}}$	Enthalpy of fusion ( $\text{KJ/mol}$ )
$\Delta H_{\text{diss}}$	Enthalpy of dissolution ( $\text{KJ/mol}$ )
$\Delta H_{\text{solv}}$	Enthalpy of solvation ( $\text{KJ/mol}$ )
$\Delta H_{\text{sub}}$	Enthalpy of sublimation ( $\text{KJ/mol}$ )
$i^*$	Number of molecules in critical nucleus

$J_{(t)}$	Nucleation Rate ( $\text{m}^{-3} \text{s}^{-1}$ )
$k$	Boltzmann constant ( $\text{J K}^{-1}$ )
$K_G$	Growth rate constant $\text{m}^{(1/m)} \text{s}^{-1}$
$K_J$	Nucleation rate constant ( $\text{m}^{-3} \text{s}^{-1}$ )
$k_n$	Nucleus numerical shape factor
$k_v$	Crystallite growth shape factor ( $\text{m}^{3-d}$ )
$m, n$	Crystallite growth exponents
$N_{\text{det}}$	Detectable number of crystallites
$q$	Cooling rate ( $\text{K s}^{-1}$ )
$q_0$	Parameter in the uc ( $q$ ) dependence for both PN and IN ( $\text{K s}^{-1}$ )
$r^*$	Critical nucleus radius (m)
$S$	Supersaturation ratio
$\Delta S_{\text{fus}}$	Entropy of fusion ( $\text{kJ/ K}^{-1} \text{mol}^{-1}$ )
$\Delta S_{\text{diss}}$	Entropy of dissolution ( $\text{kJ/ K}^{-1} \text{mol}^{-1}$ )
$T_0$	Temperature at which crystallites are instantaneously nucleated (K)
$T_C$	Crystallisation temperature (K)
$T_{\text{dis}}$	Dissolution temperature (K)
$T_e$	Equilibrium dissolution temperature (K)
$\Delta T_c$	Critical undercooling for crystallisation (K)

$T_m$	Melting point (K)
$u$	Relative undercooling
$u_c$	Relative critical undercooling for crystallisation
$v_0$	Volume of solute molecule in crystal ( $m^3$ )
$V$	Volume of solution ( $m^3$ )
$x$	Molar fraction
$\lambda$	Molecular latent heat of crystallisation ( J )
$\gamma$	Activity coefficient
$\gamma_{eff}$	Effective interfacial tension of crystal nucleus ( $mJ m^{-3}$ )
$z$	Zeldovich factor

### List of Abbreviations

ACN	Acetonitrile
PABA	Para Amino Benzoic Acid
EtOH	Ethanol
IN	Instantaneous nucleation
PN	Progressive nucleation
SD	Standard deviation
KBHR	Kashchiev–Borissova–Hammond–Roberts approach
MSZW	Metastable zone width

vdW	van der Waals
H-bonding	Hydrogen bonding
MD	Molecular dynamics

## References

- <sup>1</sup> Myerson, A.S., Handbook of Industrial Crystallization, 2nd edition, 2002, Butterworth-Heinemann
- <sup>2</sup> J. W. Mullin, Crystallization, 4th edn., Butterworth-Heinemann, Oxford, 2001
- <sup>3</sup> S. Parveen, R. J. Davey, G. Dent and R. G. Pritchard, Chem. Commun., 2005, 1531
- <sup>4</sup> R. A. Chiarella, A. L. Gillon, R. C. Burton, R. J. Davey, G. Sadiq, A. Auffret, M. Cioffi and C. A. Hunter, Faraday Discuss. 2007, **136**, 179
- <sup>5</sup> R. A. Granberg, C. Ducreux, S. Gracin and Å. C. Rasmuson, Chem. Eng. Sci. 2001, **56**, 2305.
- <sup>6</sup> R. J. Davey, Solvent effects in crystallization processes. In E. Kaldis (Ed.), Current topics in materials science, vol. 8. 1982, Amsterdam: North-Holland Publishing Company
- <sup>7</sup> R. A. Sullivan, R. J. Davey, G. Sadiq, G. Dent, K. R. Back, J. H. ter Horst, D. Toroz and R. B. Hammond, Cryst. Growth & Des., 2014, **14**, 2689
- <sup>8</sup> R. Davey, S. L. M. Schroeder, J. H. ter Horst, Angew. Chem., Int Ed. 2013, **52**, 2166
- <sup>9</sup> J. H. ter Horst and S. Jiang, Cryst. Growth Des., 2011, **11**, 256
- <sup>10</sup> H. Yang and Å. C. Rasmuson, Cryst. Growth Des. 2013, **13**, 4226
- <sup>11</sup> S. A. Kulkarni, S. S. Kadam, H. Meekes, A. I. Stankiewicz and J. H. ter Horst, Cryst. Growth Des. 2013, **13**, 2435
- <sup>12</sup> K. J. Roberts, J. N. Sherwood and A. Stewart, J. Cryst. Growth, 1990, **102**, 419
- <sup>13</sup> A. R. Gerson, K. J. Roberts and J. N. Sherwood, Powder Technol., 1991, **65**, 243

- <sup>14</sup> P. Meenan and K. J. Roberts, *J. Mater. Sci. Lett.*, 1993, **12**, 1741
- <sup>15</sup> A. M. Taggart, F. Voogt, G. Clydesdale and K. J. Roberts, *Langmuir*, 1996, **12**, 5722
- <sup>16</sup> L.A. Smith, K.J. Roberts, D. Machin, G. McLeod, *J. Cryst. Growth*, 2001, **226**, 158
- <sup>17</sup> J. Nyvlt, *J. Cryst. Growth*, 1968, **4**, 377–383
- <sup>18</sup> J. Nyvlt, R. Rychly, J. Gottfried and J. Wurzelova, *J. Cryst. Growth*, 1970, **6**, 151
- <sup>19</sup> N. Kubota, *J. Cryst. Growth*, 2008, **310**, 629
- <sup>20</sup> K. Sangwal, *Cryst. Res. Technol.*, 2009, **44**, 231
- <sup>21</sup> K. Sangwal, *Cryst. Res. Technol.*, 2010, **45**, No. 9, 909
- <sup>22</sup> N. A. Mitchell and P. J. Frawley, *J. Cryst. Growth*, 2010, **312**, 2740
- <sup>23</sup> D. Kashchiev, A. Borissova, R. B. Hammond and K. J. Roberts, *J. Cryst. Growth.*, 2010, **312**, 698
- <sup>24</sup> D. Kashchiev, A. Borissova, R. B. Hammond and K. J. Roberts, *J. Phys. Chem. B.*, 2010, **114**, 5441
- <sup>25</sup> D.M.C. Corzo, A. Borissova, R. B. Hammond, D. Kashchiev, K. J. Roberts, K. Lewtas and I. More *Cryst.Eng.Comm.*, 2014, **16**, 974
- <sup>26</sup> T. F. Lai and R. E. Marsh, *Act Cryst*, 1967, **22**, 885
- <sup>27</sup> R. Benali-Cherif, R. Takouachet, E. E. Bendeif and N. Benali-Cherif, *Act. Cryst C*, 2014, **3**, 323
- <sup>28</sup> S. Gracin and A. Fisher, *Act Cryst E*, 2005, **61**, 1242
- <sup>29</sup> H. Hao, M. Barrett, Y. Hu, W. Su, S. Ferguson, B. Wood and B. Glennon, *Org. Proc. Res. Dev.*, 2012, **16**, 35
- <sup>30</sup> M. Svård, F. L. Nordström, E. M. Hoffmann, B. Aziza and Å. C. Rasmuson *CrystEngComm*, 2013, **15**, 5020
- <sup>31</sup> R. A. Sullivan, R. J. Davey, *CrystEngComm*, 2015, **17**, 1015
- <sup>32</sup> S. Gracin and Å. C. Rasmuson, *Crystal Growth & Design* 2004, **4**, 1013
- <sup>33</sup> J. F. B. Black, R. J. Davey, R. J. Gowers and A. Yeoh, *CrystEngComm*, 2015, **17**, 5139

- <sup>34</sup> D. Toroz, I. Rosbottom, T. D. Turner, D. M. C. Corzo, R. B. Hammond, X. Lai and K. J. Roberts, *Faraday Discuss*, 2015, **179**, 79
- <sup>35</sup> J.M.Prausnitz, *Molecular Thermodynamics of Fluid Phase Equilibrium*, Prentice Hall inc, 1969
- <sup>36</sup> F. L. Nordström and Å. C. Rasmuson, *European Journal of Pharmaceutical Sciences*, 2009, **36**, 330
- <sup>37</sup> I. Rosbottom, K. J. Roberts and R. Docherty, *CrystEngComm*, 2015, **17**, 5768
- <sup>38</sup> D. Kashchiev, *Nucleation: basic theory with applications*, Butterworth-Heinemann, Oxford, 2000
- <sup>39</sup> D. Kashchiev and A. Firoozabadi, *J. Cryst. Growth.*, 2003, **250**, 499
- <sup>40</sup> Origin (OriginLab, Northampton, MA)
- <sup>41</sup> Crystal 16 details, <http://www.crystallizationsystems.com/en/crystal16/>
- <sup>42</sup> Malvern Instruments, Morphologi G3 details, <http://www.malvern.com/en/products/product-range/morphologi-range/morphologi-g3/>
- <sup>43</sup> H. B. Callen, *Thermodynamics and An Introduction to Thermostatistics*, 2nd ed.; Wiley: New York, 1985
- <sup>44</sup> M. C. Payne, M. P. Teter, D. C. Allen, T. A. Arias and J. D. Joannopoulos, *Rev. Mod. Phys.* 1992, **64**, 1045–1097
- <sup>45</sup> B. Hess, C. Kutzner, D. van der Spoel and E. Lindahl, *J. Chem. Theory Comput.* 2008 , **4**, 435
- <sup>46</sup> J. Wang, R.M. Wolf, J. W. Caldwell, P. A. Kollman and D.A. Case, *J. Comput. Chem.*, 2004, **25**, 1157
- <sup>47</sup> J. Wang, W. Wang, P. A. Kollman and D.A. Case, *Journal of Molecular Graphics and Modelling*, 2006, **25**, 247
- <sup>48</sup> I. Smallwood, *Handbook of Organic Solvent Properties*, Butterworth-Heinemann, Oxford, 2012
- <sup>49</sup> K. Pencheva, Ph.D. Thesis, University of Leeds, England, 2006
- <sup>50</sup> I. J. Bruno, J. C. Cole, P. R. Edgington, M. Kessler, C. F. Macrae, P. McCabe, J. Pearson and R. Taylor, *Acta Crystallogr., Sect. B: Struct. Sci.*, 2002, **58**, 389–397